Biosensors and Bioelectronics 141 (2019) 111439

Contents lists available at ScienceDirect

Biosensors and Bioelectronics

journal homepage: www.elsevier.com/locate/bios

Gold and silver bio/nano-hybrids-based electrochemical immunosensor for ultrasensitive detection of carcinoembryonic antigen

Sattar Akbari Nakhjavani[a,b], Hadi Afsharan[b], Balal Khalilzadeh[c,d], Mohammad Hossein Ghahremani[a,e,**], Sandro Carrara[f], Yadollah Omidi[b,g,*]

[a] Department of Molecular Medicine, School of Advanced Technologies in Medicine, Tehran University of Medical Sciences, Tehran, Iran
[b] Research Center for Pharmaceutical Nanotechnology, Biomedicine Institute, Tabriz University of Medical Sciences, Tabriz, Iran
[c] Stem Cell Research Center, Tabriz University of Medical Sciences, Tabriz, Iran
[d] Biosensors and Bioelectronics Research Center, Ardabil University of Medical Sciences, Ardabil, Iran
[e] Department of Pharmacology-Toxicology, Faculty of Pharmacy, Tehran University of Medical Sciences, Tehran, Iran
[f] Integrated Circuit Laboratory, École Polytechnique Fédérale de Lausanne, Switzerland
[g] Department of Pharmaceutics, Faculty of Pharmacy, Tabriz University of Medical Sciences, Tabriz, Iran

ARTICLE INFO

Keywords:
Carcinoembryonic antigen
Electrochemical immunosensor
Streptavidin-coated gold NPs
Streptavidin-coated silver NPs
Thiolated graphene oxide

ABSTRACT

Carcinoembryonic antigen (CEA) is an important oncomarker for the detection of breast cancer. For ultra-sensitive sensing of CEA with great specificity and accuracy, an innovative and reliable electrochemical immunosensor was developed using various nano-hybrids. A glassy carbon electrode (GC) was modified with thiolated graphene oxide (T-GO) to elevate the active surface area of the electrode. The streptavidin-coated gold nanoparticles (AuNPs) were used to increase the conductivity of the sensing area as well as the loading capacity of the biotinylated monoclonal antibody (mAb). A sandwich-on approach was developed to reach a low limit of detection (LOD). The biotinylated mAb, streptavidin coated silver nanoparticles (AgNPs) and horseradish peroxidase (HRP), altogether, formed the signaling probe of the proposed immunosensor. The electrochemical signal was significantly enhanced in the presence of hydroquinone (HQ) and hydrogen peroxide (H_2O_2). Under the optimized conditions, the proposed immunosensor presented an excellent performance in a linear range of 100 fg/mL to 5 pg/mL with a low detection limit of 75 fg/mL. The engineered immunosensor displayed excellent specificity for the detection of CEA even in the real human serum, upon which it is proposed for the early detection and monitoring of CEA in the clinic.

1. Introduction

Despite huge advancements in cancer treatment, breast cancer (BC) is still the most common malignancy and the second leading death-causing cancer among women worldwide. It has been estimated to be responsible for approximately 626 thousand deaths in 2018 (Bray et al., 2018). Owing to the early diagnosis and recent advances in treatment, the detection of new cases of the BC had increased while its mortality rate had been constant or even dropped during recent years (Rojas and Stuckey, 2016). Along with traditional approaches for diagnosis of BC such as mammography, radiology, CT and PET scan, which require skilled technicians, high-tech instruments and complicated facilities, developing new methods with high sensitivity, proper specificity and accessibility are highly demanded. Tumor markers such as carcinoembryonic antigen (CEA), cancer antigen 15-3 (CA 15-3), human epidermal growth factor receptor-2 (HER-2), mammaglobin and cytokeratins perform a significant role in the early detection, screening, monitoring of recurrence and treatment of BC (Aktas et al., 2016; Stieber et al., 2015; Svobodova et al., 2018; Zehentner and Carter, 2004). In comparison with common and routine indexes such as tumor size, lymph node status, and tumor grade, which gathered with high-tech and complex devices, the aforementioned biomarkers are very accessible and non-invasive. Among various biomarkers, CEA has extensively been used in the clinical field for many years. CEA, a serum glycoprotein, belongs to the superfamily of immunoglobulins and has overexpressed in the several types of cancers, including BC (Thompson et al., 1991). CEA has effectively used in the monitoring and management of breast cancer recurrences for many years and it counts as one of the two key biomarkers for early detection of the BC relapse, even before the appearance of clinical and radiological symptoms of the

* Corresponding author. Research Center for Pharmaceutical Nanotechnology, Biomedicine Institute, Tabriz University of Medical Sciences, Tabriz, Iran.
** Corresponding author. Department of Molecular Medicine, School of Advanced Technologies in Medicine, Tehran University of Medical Sciences, Tehran, Iran.
E-mail addresses: mhghahremani@tums.ac.ir (M.H. Ghahremani), yomidi@tbzmed.ac.ir (Y. Omidi).

https://doi.org/10.1016/j.bios.2019.111439
Received 6 April 2019; Received in revised form 2 June 2019; Accepted 14 June 2019
Available online 19 June 2019
0956-5663/

disease (Shao et al., 2015; Wu et al., 2014; Zaleski et al., 2018). Therefore, the ultra-sensitive techniques for determination of trace changes in the CEA concentration of the serum of patients are highly required. This can be greatly useful in terms of the tumor relapse diagnosis as well as the treatment strategy in the management of the disease progression. Different routine procedures have so far been introduced for the detection of CEA such as fluorescent labeling, enzyme-linked immunosorbent assay (ELISA), radio-immunoassay (RIA) and enzyme immunoassay (EIA) (Ogoshi and Mitomi, 1984; Orjasaeter et al., 1985; Wu et al., 2003). Although the aforementioned approaches represented relatively appropriate and sensitive detective tool for the monitoring of CEA, developing more highly-sensitive and -specific methods seem to be necessary. To tackle such shortcomings, electrochemical (EC) immunosensors have attracted the attention of researchers, in large part because of offering a number of benefits, including simplicity, being user-friendly, cost- and time-effectiveness, fast response time and very low detection limits (LODs). Immunosensors are envisioned to become robust sensing and monitoring tools for the detection of various oncomarkers, in large part because of (i) being simple and cost-effective in terms of development, (ii) providing a great possibility for efficiently sensitive and specific detection of molecular markers, and (iii) offering suitable shelf-life. Further, they may display somewhat shortcomings such as reusability that can be resolved by the implementation of *de novo* approaches, including disposable paper-based sensors. The EC approaches have widely been used for the detection of various tumor markers (e.g. CA 125, CA 15-3, p53, microRNA) and analytes (e.g., anesthetics, pesticides, anticancer drugs) with high sensitivity (Afsharan et al., 2016; Aliakbarinodehi et al., 2016; Khalilzadeh et al. 2015, 2019; Mohammad et al., 2018; Samadi Pakchin et al., 2018). The recent improvements in nanotechnology and the use of advanced nanomaterials such as carbon-based materials and metal nanoparticles (NPs) have revolutionized the engineering of biosensors with extremely low LODs (Ahmad and Mobin, 2019; Aliakbarinodehi et al., 2018; Babamiri et al., 2018; Khalilzadeh et al. 2011, 2016). Because of the unique physicochemical characteristics (e.g., large active surface area and high stability) of metal NPs such as gold and silver (AuNPs and AgNPs, respectively), they have widely been used in the engineering of sensors. Additionally, their excellent conductivity rationalizes their application in the modification of biosensors (Zeng et al., 2011). Of these materials, graphene, a two-dimensional nanomaterial synthesized from graphite, has been applied in the development of biosensing and sensing devices (Ahmad et al., 2016; Khalilzadeh et al., 2016; Tzouvadaki et al., 2018). It has been considered a leading agent for the enhanced sensing, in large part because of its remarkable properties such as incredible conductivity (15,000 cm2/V s), large surface area (supposedly 2630 m^2/g), low cost, exceptional chemical stability and good water dispersibility (Cao et al., 2018; Rahmanian et al., 2017; Roy et al., 2011; Song et al., 2016; Zhu et al., 2017).

In this study, we aimed to design and develop an electrochemical immunosensor for the ultra-sensitive detection of CEA which is an important oncomarker in breast cancer. In fact, given the high costs of the currently used conventional diagnostic methods, which often lack early and on time detection potential, the use of cost-effective and highly sensitive immunosensors with great accuracy may result in improved diagnosis and hence health statistics such as survival rate of patients. To achieve maximum sensitivity, we employed various strategies. First, the electrode surface was modified with thiolated-GO to increase the active surface area of the electrode. Second, AuNPs were coated with streptavidin and introduced to the electrode surface to increase the active surface of the immunosensor, which also enhanced the loading capacity of CEA monoclonal antibody (mAb) on the electrode surface. Third, a sandwich approach was implemented to reach the highest sensitivity using streptavidin-coated AgNPs conjugated with CEA mAbs. Finally, the horseradish peroxidase (HRP) was used to amplify the obtained electrochemical signals. To attain the maximum sensitivity, H_2O_2 was applied in the sensing analyte. In harmony with this design, for the first time, the engineered biosensor resulted in excellent sensitivity and specificity, which is proposed for the ultra-sensitive and early detection of CEA in breast cancer relapse.

2. Experimental

All materials list, procedures, and apparatus have fully been described in the Supplementary Materials.

2.1. Synthesizing of AuNPs and AgNPs

Turkevich method was employed for synthesizing AuNPs as described here with slight modification (Zhang and Cui, 2009). First, $HAuCl_4$ (27 mg) was added to 100 mL boiling distilled water (DW) and stirred for 40 min. Then, 4.5 mL of trisodium citrate 1% (w/v) was added to the mixture and refluxed for 45 min. The color of the solution changed from yellow to wine red during this process. After cooling down to room temperature (RT) and filtration, the AuNPs were obtained. Preparation of AgNPs was carried out using a previously reported method with a minor alteration (Mulfinger et al., 2007). In brief, 10 mL of 2.0 mM $NaBH_4$ solution was chilled in ice water, then 10 mL of 1.0 mM $AgNO_3$ solution was added dropwise while the mixture was vigorously stirring. After the addition of the whole silver nitrate solution, the color of the solution changed to yellow and then the stirrer was moved away. The obtained AgNPs were characterized and kept in RT for applications.

2.2. Synthesis of graphene oxide and its thiol modification

Graphene oxide (GO) was prepared using Hummer's method with some modifications (Marcano et al., 2010). Briefly, 2.0 g of graphite and 1.0 g of $NaNO_3$ were added into 46 mL concentrated H_2SO_4 chilled and stirred in an ice bath for 30 min. Then 6.0 g of $KMnO_4$ was added into the solution and stirred for another 30 min in the warm water. Afterward, 92 mL of water was added to the solution, and the temperature increased up to 95-98 °C. After 50 min of stirring, the solution transferred into an ice bath and 280 mL of water and 4 mL of H_2O_2 were added and stirred for 20 min. Then, the obtained mixture cooled at RT and purified (filtration, multiple washing, centrifugations, and vacuum drying) for the characterization. To prepare T-GO, 135 mg of GO dispersed in 13.5 mL of DW using sonication bath for 20 min. Meanwhile, 2.25 g Na_2S was dissolved in 3 mL DW and then added into the solution. The whole reaction was stirred overnight at 55 °C under reflux condition. After that, the mixture was washed and centrifuged several times to collect black sediment. After drying at 40 °C, T-GO was obtained (Kim et al., 2012).

2.3. Preparation of streptavidin-coated NPs

Briefly, 2 mL of synthesized AuNPs and AgNPs were separately mixed with 90 µL streptavidin (1 mg/mL) and stirred at 37 °C for 40 min. Then, BSA was added to the solution to prevent the non-specific binding. The mixture was centrifuged and stored at 4 °C.

2.4. Preparation of signaling label

The signaling label of proposed CEA immunosensor was prepared before its use. Briefly, 10 µL of streptavidin-modified AgNPs and 10 µL mAb were incubated at 37 °C for 1 h. The mixture was incubated at 37 °C in the presence of 10 µL of biotinylated HRP for 25 min with 100% humidity. To reach the maximum conjugation rate, during both incubations, the mixture was gently mixed.

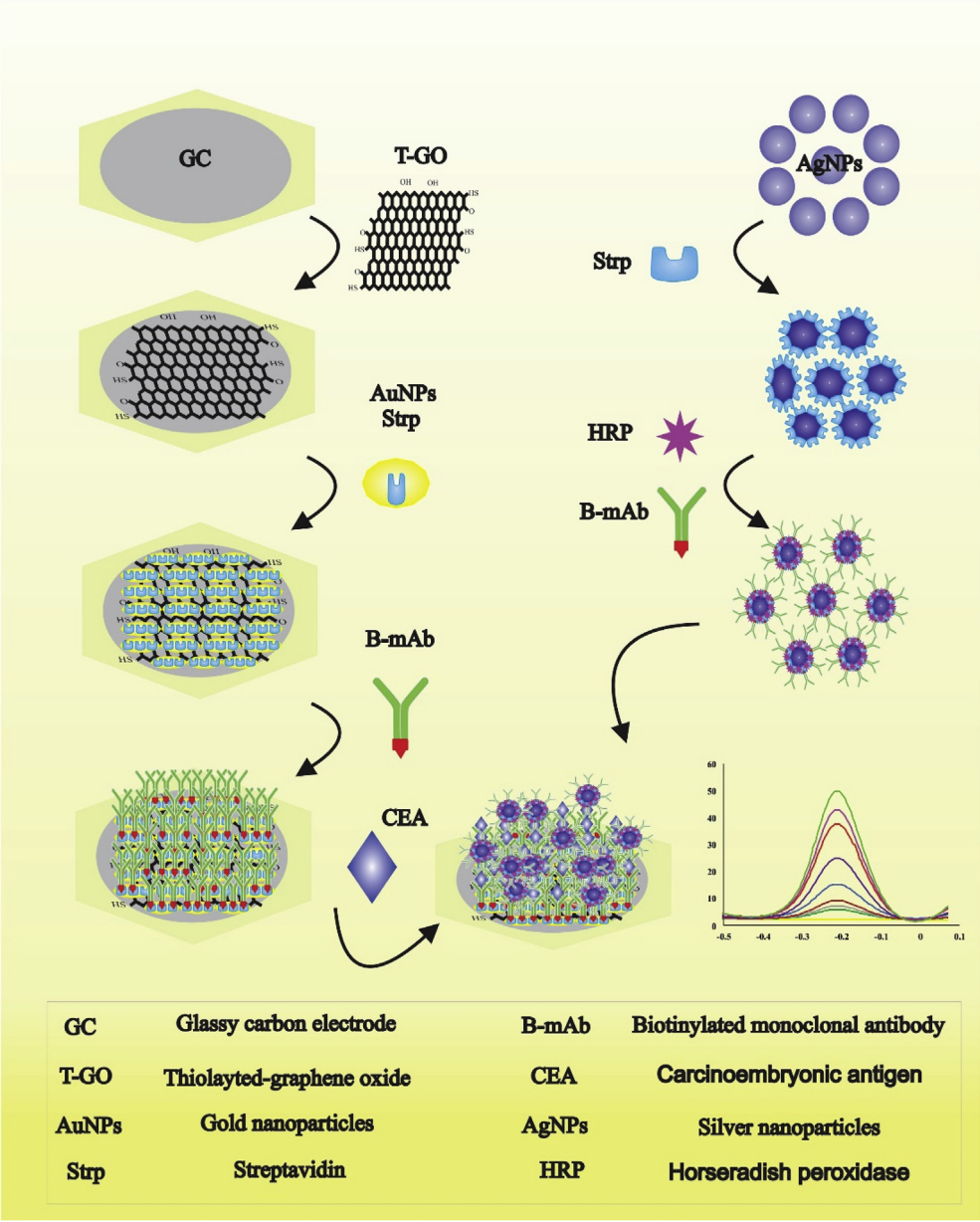

Scheme 1. Graphical illustration of the CEA immunosensor fabrication. T-GO was cast on the GC electrode, then strp-AuNPs were introduced. After immobilizing of mAb, the CEA was introduced. A sandwich signaling probe containing HRP-(strp-AgNPs)-mAb was applied for ultrasensitive detection of CEA.

2.5. Electrode modification and preparation of the CEA immunosensor

As illustrated in Scheme 1, the modification of the electrode was done as follows: first, the glassy carbon electrode (GC) was polished on a pad with alumina powder and washed with water to completely clean the surface. Next, T-GO (10 µL, 1.5 mg/mL) was drop-casted on the GC and stayed at RT until dried. To further modify the electrode, 10 µL of streptavidin modified AuNPs were dropped onto the GC/T-GO and incubated at 4 °C for almost 3 h. Then, the electrode was immersed in a solution of capture antibody and stored at 4 °C for 6 h with 100% humidity. BSA (1% w/v) was then used to minimize the non-specific bindings. The GC/T-GO/AuNPs/Ab1 modified electrode was next soaked in the desired concentration of CEA protein for 60 min and washed afterward with PBS. To complete the sandwich procedure in preparation of CEA biosensor, 10 µL of the as-prepared signaling label was cast on the surface of the modified electrode and incubated at 37 °C for 60 min with 100% humidity. The CEA protein and antibodies were kept at RT for 10 min before their use. The electrochemical detection procedures were done using the modified electrode, as a working electrode, with different concentration of CEA in PBS (0.1 M, pH7.0) containing HQ and H_2O_2.

3. Results and discussion

3.1. Characterization of synthesized nanomaterials

Various techniques were applied to characterize the fabricated nanostructures, including field emission scanning electron microscopy (FE-SEM), transmission electron microscopy (TEM), Raman spectroscopy, X-ray diffraction (XRD), Fourier transforms infrared (FTIR) and ultraviolet-visible spectroscopy (UV-Visible). The SEM micrographs of AuNPs and streptavidin-coated NPs revealed a spherical shape with proper distribution for AuNPs, while the morphology of the NPs showed some changes mainly because of the NPs modification with streptavidin (Fig. 1a and b). The SEM image of AgNPs (Fig. 1d) showed round-shape particles while the streptavidin-coated particles (Fig. 1e) presented

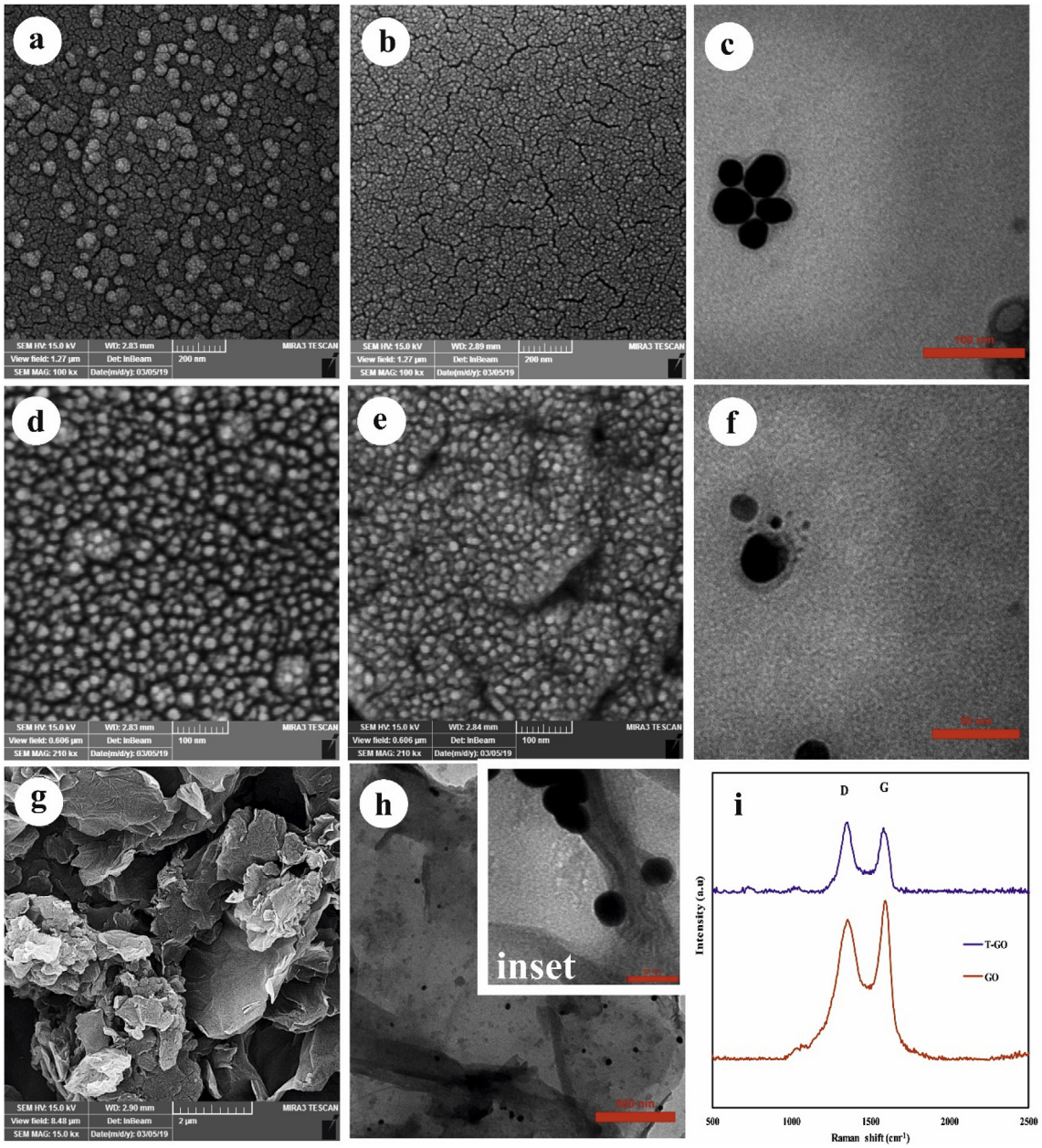

Fig. 1. Characterization of constructed nanostructures; (a) SEM micrograph of synthesized AuNPs. (b) SEM micrograph of streptavidin-coated AuNPs. (c) TEM micrograph of streptavidin-coated AuNPs. (d) SEM micrograph of prepared AgNPs. (e) SEM micrograph of streptavidin-coated AgNPs. (f) TEM micrograph of streptavidin-coated AgNPs. (g) SEM micrograph of T-GO. (h) TEM micrographs of T-GO with streptavidin-coated AuNPs; Inset: maximized streptavidin-coated AuNPs on the T-GO. (i) Raman spectra of synthesized GO and its thiolation, i.e. T-GO.

morphological alteration due to their modification with streptavidin. As shown in Fig. 1, the TEM micrographs of streptavidin-coated gold and silver NPs revealed a successful modification of NPs (i.e., the corona around NPs). Furthermore, to demonstrate the successful synthesis of NPs and their modification with streptavidin, UV-Visible spectroscopy was employed. In this regard, the UV-Visible analysis of AuNPs and AgNPs revealed some changes compared to the streptavidin-coated NPs. As described in Fig. S1a, and considering the surface plasmon of AuNPs, they showed a peak around 525 nm (Zhang and Cui, 2009), while another peak appeared around 273 nm indicating successful installation of streptavidin on the AuNPs upon their modification with streptavidin (Vandghanooni et al., 2018). This phenomenon also observed while the AgNPs were equipped with streptavidin (Fig. S1b). Interestingly, the UV-Visible peak of AgNPs was found around 396 nm (Mulfinger et al., 2007), while another peak was detected around 270 nm after their modification with streptavidin (Vandghanooni et al., 2018). The morphology of synthesized and modified T-GO was portrayed in Fig. 1h, demonstrating a layer-shape and crumpled construction. The TEM micrographs of T-GO with streptavidin-coated AuNPs displayed a successful modification of T-GO with AuNPs (Fig. 1h). The XRD patterns of GO and T-GO were illustrated in Fig. S1c. As expected, the GO presented a sharp peak at $2\Theta = 9.8^{\circ}$ due to complete oxidation of graphite. After successful thiolation of GO, the peak was shifted to around $2\Theta = 24^{\circ}$ (Orth et al., 2013). Raman spectroscopy was applied to study the structural modifications of the T-GO following its thiolation process. As illustrated in Fig. 1i, the characteristic D bands for GO and T-GO, related to oxidizing defects, respectively occurred at 1356 and 1350 cm^{-1}, while the G bands, which correspond C–C stretching on the graphite structure (Dresselhaus et al., 2010), recorded at 1592 and 1582 cm^{-1}, respectively. The intensity ratio of D and G bonds was used

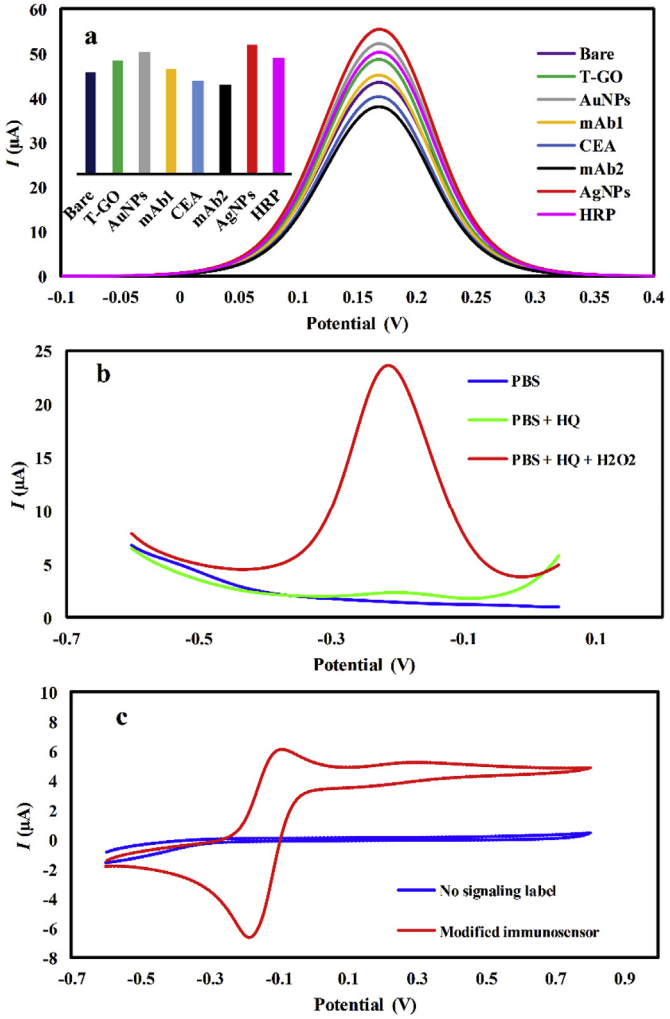

Fig. 2. Evaluation of the immunosensor preparation steps. (a) DPV voltammograms of preparation steps in PBS, containing 5 mM K3 [Fe (CN) 6]/K4 [Fe (CN) 6] (1:1) and KCl (0.1 M). Inset: peak current changes during modification steps. (b) Analysis of the effect of HQ and H_2O_2 on the performance of immunosensor in PBS. (c) Analysis of sandwich formation and its effect on the performance of immunosensor in PBS (containing HQ and H_2O_2). DPV: Differential pulse voltammetry.

to examine the degree of the functionalization. On the other words, following the thiolation of GO, the ID/IG ratio of GO increased from 0.88 to 1.02 for T-GO, indicating a successful establishment of thiol groups on the GO (Orth et al., 2013). To assess the structural alteration of T-GO, the FTIR spectroscopy was applied. Having compared the T-GO FTIR spectrum with GO (Fig. S1d), some changes were found in the spectra, that is, the appearance of a peak around 2550 to 2650 cm^{-1} due to presence $S-H$ groups which showed the successful thiolation of GO (Orth et al., 2013).

3.2. Electrochemical characterization of the engineered CEA immunosensor

Electrochemical characterizations were performed to authenticate the reliability of proposed-engineered CEA immunosensor. In this regard, differential pulse voltammetry (DPV), as a sensitive electrochemical technique, was conducted to monitor the electrochemical preparation of CEA immunosensor. DPV voltammograms of various steps of CEA electrode modification were accomplished in the PBS (0.1 M, pH = 7.5) containing 5 mM K3 [Fe (CN) $_6$]/K4 [Fe (CN) $_6$] (1:1) and KCl 0.1 M. As shown in Fig. 2a, the peak current of bare GC was amplified following modification of the electrode surface with T-GO, which associates with an increase in the conductivity and active surface area of the electrode. To intensify the EC signal, AuNPs were added on the surface of the modified electrode. The obtained current showed a satisfactory level, attributable to the acceleration of electron transfer in comparison with that of the bare electrode. This may directly associate with the attachment of AuNPs on the T-GO modified electrode. By casting the primary CEA mAb and its immobilization on the surface of the modified electrode, the peak current meaningfully decreased. This incident would be elucidated by the increase in the resistance of the electrode surface as a result of the attachment of mAb on the AuNPs. The declining trend in the current continued by the introducing of CEA protein. It worth explaining that the signaling label was evaluated individually. In other words, to evaluate the correctness of preparation steps of designed immunosensor, the components of the signaling label were separately introduced. Following the incubation of the secondary mAb on the immunosensor, the decrease in the peak current observed. This phenomenon could be interpreted by insulator behavior of both CEA protein and the secondary mAb, which led to an interference with the electron transfer procedure. Therefore, the peak current dramatically diminished, which indicates the formation of a sandwich of mAb-CEA-mAb and successful development of the immunosensor. To this end, after introducing streptavidin-AgNPs, the electrochemical performance of the immunosensor was advanced, in large part due to the facilitation of electron transfer in the sensing environment. Significant growth of the fallen peak current demonstrated that the streptavidin-AgNPs were efficiently attached to the capture mAb. Expectedly and after adding the HRP, the immunosensor displayed a decrease in the electrochemical peak current, which verifies the successful immobilization of HRP (Fig. 2a, inset).

3.3. Electrochemical principals of the proposed CEA immunosensor

As a well-established fact, applying electron mediators such as thionine, methylene blue, and hydroquinone (HQ) in the sensing strategies could effectively influence the performance of the immunosensor by amplifying the electrochemical signals. In this regard, to improve the performance of the electrochemical biosensor, different enzymes with the catalytic activity have also been used, including alkaline phosphatase, lactate oxidase, horseradish peroxidase (HRP) and glucose oxidase (Pakchin et al., 2017). Profiting the catalytic activity of nominated enzymes, HRP was chosen to enhance the sensitivity of our proposed CEA immunosensor, while HQ acted as an electron mediator. It should be noted that the electrochemical reduction of HQ can be hastened in association with H_2O_2. The electrochemical reduction of HQ in the presence of H_2O_2 and engineered CEA immunosensor with HRP, as illustrated in reaction 1 (Akbari Nakhjavani et al., 2018).

Reaction 1:

$$HRP\ (Fe^{3+}) + H_2O_2 \rightarrow HRP\ (Fe^{4+}) + H_2O$$

$$HRP\ (Fe^{4+}) + HQ_{(red)} \rightarrow HRP\ (Fe^{3+}) + HQ_{(ox)}$$

$$HQ_{(ox)} + 2H^+ + 2^{e-} \rightarrow HQ_{(red)}$$

3.4. Electrochemical behavior of the engineered CEA immunosensor

The electrochemical response of proposed CEA immunosensor was investigated by two different approaches. Initially, the interaction of HQ and HRP was considered in the presence of H_2O_2. The modified CEA immunosensor was electrochemically examined in PBS (pH 7, 0.1 M) using DPV technique. The results showed no significant changes in the peak current with linear voltammograms. The measurement was repeated following the adding of HQ, as an electron mediator. The voltammograms demonstrated a small change in the peak current, which might be associated with the enzymatic activity of HRP in the HQ reduction process. By the injection of H_2O_2 into the measurement media,

the peak current significantly raised. In fact, in the presence of H_2O_2, the HRP attached on the CEA immunosensor can cause an acceleration in the electron transfer in the electrode surface and accordingly the electrochemical response of immunosensor meaningfully can be elevated. Taking all these into consideration, it could be summarized that the maximum electrochemical response of the proposed engineered CEA immunosensor happened in the presence of both HQ and H_2O_2 (Fig. 2b). The second approach was to evaluate the performance of the CEA immunosensor in the absence of its signaling label. The obtained data revealed a meaningless peak current in the working cell environment, i.e., PBS (pH 7, 0.1 M), HQ, and H_2O_2. By completing the sandwich assay in the presence of the signaling label, the peak current (Fig. 2c.) showed a growth, which indicates that the signaling label used can efficiently capture its target.

3.5. Optimization of experiment conditions

To guarantee the best performance of the proposed CEA immunosensor, various experimental parameters were initially optimized, which potentially could influence the quality of signals of the biosensor. To improve the performance of the developed immunosensor for the electrochemical detection of CEA, various factors (i.e., pH, the concentration of HQ and H_2O_2) were optimized.

The quality and quantity of electrochemical signals of the engineered CEA immunosensor were influenced by the pH of the electrochemical cell media. Therefore, the effect of pH was initially optimized using SWV and DPV techniques. The modified immunosensor was fabricated using 2 pg/mL of CEA and was evaluated in PBS containing 1 mM HQ and 1 mM H_2O_2 with various pHs (varying from 5 to 9.5). Along with the increased pH, the obtained peak currents started to grow, while the peak currents reached their maximum amount around the pH of 7. Further elevation of pH (up to 9.5) led to a drop in the height of the peak currents associated with a decrease in the response of immunosensor. The data analysis revealed that at the pH of 7, the proposed immunosensor responded to its best performance. Hence, the pH 7 was selected to continue the experiments (Fig. 3a), which was in great consensus with previously reported electrochemical biosensors (Akbari Nakhjavani et al., 2018; Zhao et al., 2011).

As the next parameter, the concentration of HQ was optimized to evaluate its impact on the electrochemical peak currents of the modified immunosensor. Because of the excellent electrochemical behavior of HQ as an electron mediator, its application in the development of biosensors has been reported (Akbari Nakhjavani et al., 2018; Torrente-Rodríguez et al., 2015). Therefore, the impact of HQ concentration on the performance of the CEA immunosensor was studied using both the DPV and SWV methods in the PBS (pH 7, 0.1 M) containing various amounts of HQ (0–3.6 mM) and constant concentration of 1 mM H_2O_2. The CEA immunosensor presented an increasing trend when the HQ concentration reached 2.3 mM before the electrochemical currents began to fall. The amount of 2.3 mM shows a proper similarity in comparison with the previously reported works (Zhao et al., 2011). As a result, it selected as the optimum concentration of HQ (Fig. 3b).

The concentration of H_2O_2, as a factor which influences the electrochemical response of the CEA immunosensor, was also optimized. Accordingly, the modified CEA immunosensor was evaluated by the SWV and DPV techniques in PBS (pH 7, 0.1 M) containing 2.3 mM HQ and different amounts of H_2O_2 (0–3.1 mM). Based on the results illustrated in Fig. 3c, the response of engineered immunosensor was interestingly increasing. At the concentration of 1.8 mM, the height of the peak current touched its maximum. By increasing the concentration of H_2O_2, the significant elevation of the electrochemical response of the CEA immunosensor vanished. Therefore, the concentration of 1.8 mM was considered as the optimum amount of H_2O_2.

3.6. Detection of CEA with the proposed immunosensor

The as-prepared CEA immunosensor, i.e., GC/T-GO/strp-AuNPs/mAb/CEA/mAb/strp-AgNPs/HRP, with various amounts of CEA was electrochemically investigated using DPV technique. Considering the results (Fig. 4a), the proposed CEA immunosensor showed an excellent association with the amount of CEA under the optimized conditions. In other words, along with the increase of the CEA concentration, the electrochemical response of the engineered CEA immunosensor dramatically was increased due to the more interaction of signaling label, that is, mAb2/strp-AgNPs/HRP with the analyzing electrolyte that contains HQ and H_2O_2. The electrochemical CEA immunosensor demonstrated outstanding performance in a linear range between 0.1 to 5 pg/mL. The linear relation of CEA immunosensor response for the electrochemical detection method was illustrated by the equation of I (μA) = 8.9889 CEA concentration (pg/mL) +3.4036 with a coefficient correlation of 0.99 (Fig. 4b). The LOD and limit of quantification (LOQ) of the proposed electrochemical CEA immunosensor were calculated as 75 fg/mL and 250 fg/mL at a signal to noise ratio of 3 and 10, respectively. The obtained results revealed that the proposed electrochemical CEA immunosensor showed an excellent sensitivity towards detection of CEA in comparison with previously reported studies (Table 1). Thus, it could be explained that by the strategies used, the electrochemical signals can be significantly enhanced even for very low concentrations of CEA. As the first approach to amplify the EC signals, the electrode surface, and the conductivity were enormously increased using GO. Secondly, the strp-AuNPs was used to enhance not only the aforementioned concepts but also the loading capacity for attaching of the primary antibody, in large part because of the unique structure of streptavidin that offers four times more binding sites (Zhu et al., 2015).

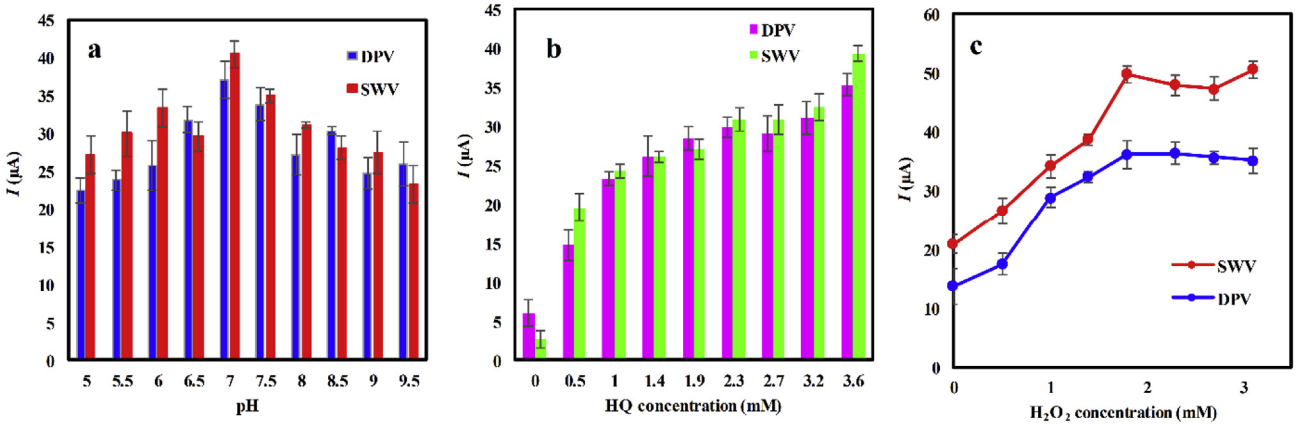

Fig. 3. Optimization of experimental conditions for the proposed CEA immunosensor. (a) The peak currents of various pHs. (b) The optimization of HQ concentration in optimized pH. (c) The optimization of H2O2 concentration in the presence of optimum pH (7.0) and HQ concentration (2.3 mM).

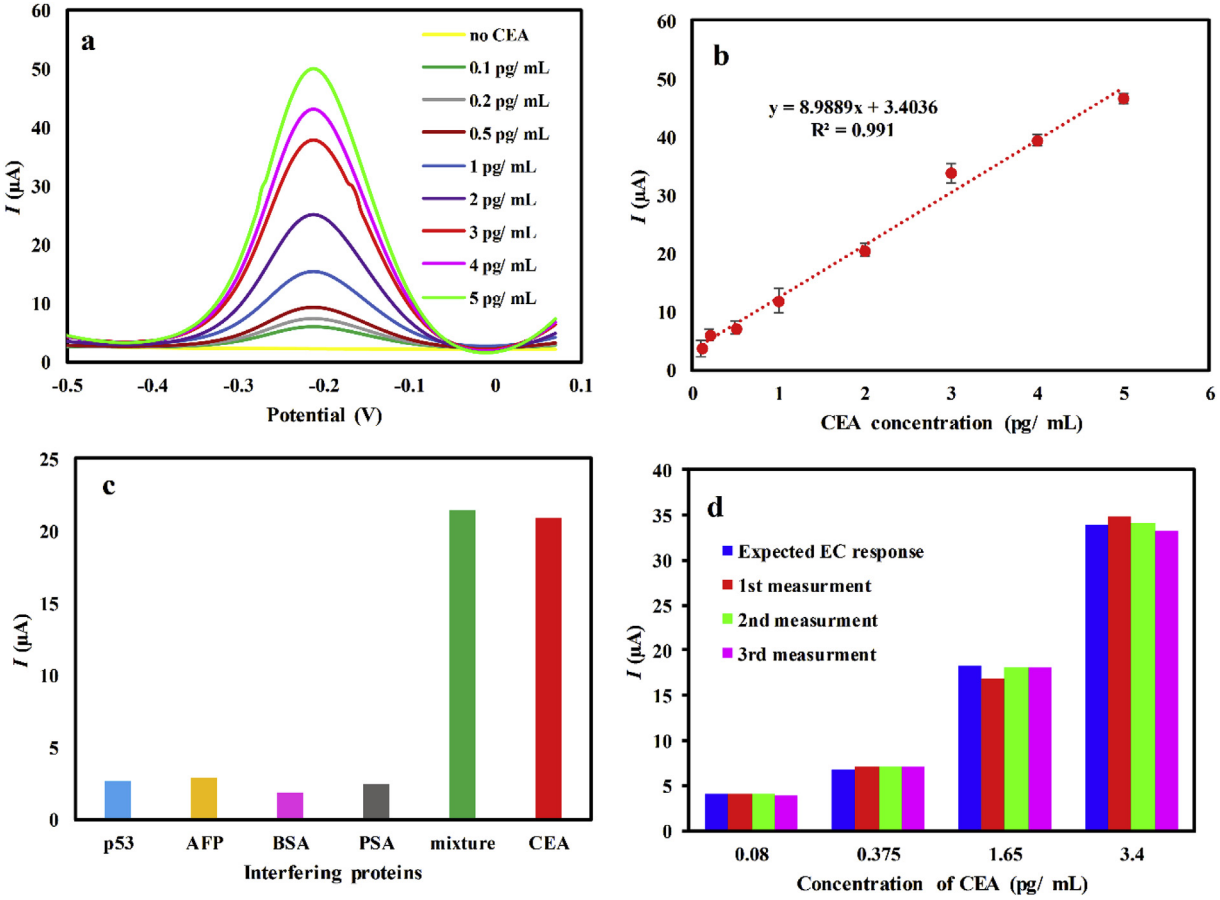

Fig. 4. Evaluation of the immunosensor performance. (a) The DPV voltammograms of immunosensor modified using various concentrations of CEA. (b) The current response of immunosensor toward various amounts of CEA and the related calibration curve. (c) Interfering investigation of proposed immunosensor in the presence of different interferes. (d) The performance of the CEA immunosensor in real human serum samples containing different concentrations of CEA.

Additional signal enhancement ensured by employing streptavidin coated AgNPs in the signaling label, the sandwich part, which boosts the loading capacity of secondary mAb and electrochemical conductivity of designated CEA immunosensor. Meanwhile, the sandwich label was armed with HRP to attain the extreme electrochemical signal amplification. Final signal amplification was obtained due to equipping the analyzing solution with HQ and H_2O_2, which efficiently improved the electrochemical signals of the CEA immunosensor. Having applied the aforementioned strategies, the constructed CEA immunosensor presented an excellent performance in the detection of CEA oncomarker.

3.7. Stability, specificity, and repeatability of the CEA immunosensor

Practical stability oftentimes is considered as one of the main factors to investigate the performance of a detection system. In this regard, the storage stability of the CEA immunosensor was evaluated in the optimized conditions. To this end, the engineered CEA immunosensor was

Table 1
Comparison of the proposed immunosensor with the previously reported immunosensors for the detection of CEA.

Electrode modification	Method	Linear range	LOD	Ref.
GC/G-NF/MB/AuNPs/Ab/CEA	DPV	0.5–120 ng mL^{-1}	170 pg mL^{-1}	Li et al. (2011)
GC/Strp-CS-NG/biotin-Ab1/CEA/HRP-Ab2	DPV	0.02–12 ng mL^{-1}	10 pg mL^{-1}	Yang et al. (2017)
CPE/TiO2/(CS + AuNPs)-Ab	DPV	0.01–1 and 1–20 ng mL^{-1}	10 pg mL^{-1}	Aslan and Anik (2014)
Au/ZnO NPs/AuNPs/anti-CEA/HRP	SWV	0.1 to 70 and 70–200 ng mL^{-1}	10 pg mL^{-1}	Norouzi et al. (2011)
CdS@Rh123-Ab2/CEA/Ab1/GO-MoS2/ITO	PEC	10 pg.mL^{-1}- 80 ng mL^{-1}	3.2 pg mL^{-1}	Song et al. (2018)
GC/PPDNS/HRP-Ab/CEA	DPV	0.01–60 ng mL^{-1}	3.2 pg mL^{-1}	Xu et al. (2015)
ITO/PANI/PPy-Ag/Ab1/CEA/Ab2- ZnO@AgNCs	ECL	10^{-3} -100 ng mL^{-1}	0.4 pg mL^{-1}	Zhang et al. (2017)
GC/NH2-GS/Ab1/CEA/PdPt nanocages/MWCNT-NH2-Ab2	Amp	0.001–20 ng mL^{-1}	0.2 pg mL^{-1}	Li et al. (2015)
GC/Au@PDA/Ab1/Au@PtDNs/NG/Cu^{2+}-Ab2	Amp	0.5 pg.mL^{-1}- 50 ng mL^{-1}	167 fg mL^{-1}	Lv et al. (2018)
GC/GO-CS/Ab/CEA/Apt-AuNPs	SWV	0.5 pg.mL^{-1}- 1 ng mL^{-1}	100 fg mL^{-1}	Jiang et al. (2017)
GC/T-GO/Strp-AuNPs/Ab1/CEA/Strp-AgNPs-HRP/Ab2	DPV	0.1–5 pg mL^{-1}	75 fg mL^{-1}	Current work

GC: glassy carbon electrode, G-NF: graphene-nafion composite, MB: methylene blue, Ab: antibody, DPV: differential pulse voltammetry, Strp: streptavidin, CS: chitosan, NG: nitrogen-doped graphene, CPE: carbon paste electrode, TiO2: titanium oxide, SWV: square wave voltammetry, CdS: dadmium sulfide, Rh123: rhodamine 123, GO: graphene oxide, MoS2: Molybdenum disulfide, ITO: Indium Tin Oxide, PEC: photo-electrochemical, PPDNS: poly(o-phenylenediamine) nanospheres, PANI/PPy-Ag: polyaniline/polypyrrole-sliver, ECL: electrochemiluminescence, GS: graphene sheets, Pd: palladium, Pt: platinum, MWCNT: multi-walled carbon nanotube, Au@PDA: gold nanoparticles functionalized polydopamine (Au@PDA), Au@PtDNs: Gold@platinum dendritic nanomaterials, Cu: copper, Amp: amperometry, Apt: aptamer, NG: nitrogen-doped graphene, T-GO: thiolated graphene oxide, AgNP: silver nanoparticle.

stored in PBS (pH 7.4, 0.1 M) at 4 °C for two weeks. The results indicated that the proposed CEA-detecting immunosensor displayed similar responses based on its initial signal (90% of its original performance), which seems to be in good consensus with some previous studies using carbon materials and metal NPs for the development of biosensors (Li et al., 2015; Lv et al., 2018). Our findings indicated that the engineered CEA immunosensor possessed excellent storage stability; nonetheless, some graphene-based immunosensors were reported to present slightly better storage stability (Song et al., 2018; Yang et al., 2017).

The specificity of an immunosensor should be evaluated to suggest it as a proper tool for the detection of tumor biomarkers. In this regard, the selectivity of the engineered CEA immunosensor was validated in the presence of different interferences, including prostate-specific antigens (PSA), bovine serum albumin (BSA), p53, α-fetoprotein (AFP) and their mixture with CEA. To investigate the effect of interferences on the performance of our immunosensor, the DPV technique was performed with the CEA immunosensor modified with 10 ng/mL BSA, 50 ng/mL PSA, 100 ng/mL p53, 100 ng/mL AFP, 2 pg/mL CEA and their mixture. As demonstrated in Fig. 4c, the engineered CEA immunosensor was not influenced by various interfering proteins, presenting excellent specificity and selectivity for the detection of CEA. The repeatability of the proposed CEA immunosensor was also studied. To this end, the CEA immunosensor was modified with 2 pg/mL CEA and was investigated by repeating measurements (n = 5). The obtained results indicated an acceptable precision for the engineered CEA immunosensor (RSD 3.7%).

3.8. Detection of CEA in real samples

The possibility of the practical application of fabricated CEA immunosensor was validated by recovery experiments. The real human serum samples were prepared using the standard addition method. The as-prepared spiked samples were used to fabricate the CEA immunosensor. The results were calculated by the obtained regression equations (Table 1S). According to these results, besides the results of repeated measurements illustrated in Fig. 4d, the engineered CEA immunosensor demonstrated marked performances for the detection of CEA in the human serum. Therefore, the proposed immunosensor could be potentially considered for the ultra-sensitive detection of CEA in the clinic.

4. Conclusion

Here, for the first time, we developed an exceptional electrochemical immunosensor for the detection of CEA oncomarker. To maximize the sensitivity of the proposed immunosensor, the sandwich strategy was employed benefiting from advanced nanomaterials to enhance the performance of the immunosensor. In short, T-GO was applied to enhance the surface area of the electrode and also to improve the conductivity of the electrode. In addition, AuNPs coated with streptavidin provided more oriented binding sites for biotinylated mAb, and hence, a dense-loading capacity for mAbs. The same enhancement strategy was applied in the sandwich labels, consisting of AgNPs coated with streptavidin. Having used streptavidin, the signaling probe was further modified with HRP accompanied by a secondary mAb to markedly intensify the signals. As the final step in the amplification of the signals, the analyzing media was enriched with HQ and H_2O_2, which influenced the electrochemical signals by providing and facilitating electron transfer in the measurement environment. The engineered immunosensor displayed a wide linear detection range and an excellent LOD/LOQ, compared to the previously reported studies (Table 1). Furthermore, the engineered immunosensor presented significantly great stability, repeatability, specificity, and selectivity. Considering the great potential of the engineered immunosensor in the detection of CEA in the real serum samples, this immunosensor is proposed to be used for the ultra-sensitive detection and monitoring of the CEA oncomarker in the blood samples of patients with breast cancer.

Declaration of interests

The authors declare that they have no known competing financial interests or personal relationships that could have appeared to influence the work reported in this paper (entitled “Gold and silver bio/nano-hybrids-based electrochemical immunosensor for ultrasensitive detection of carcinoembryonic antigen”).

Ethical issues

This study was ethically approved (IR.TUMS.REC.1394.1273) by Tehran University of Medical Sciences (Tehran, Iran). All human samples were collected with patients’ consent by signed forms.

Conflict of interests

The authors have no conflict of interest to declare relevant to this article.

CRediT authorship contribution statement

Sattar Akbari Nakhjavani: Conceptualization, Formal analysis, Writing - original draft, Writing - review & editing. **Hadi Afsharan:** Formal analysis. **Balal Khalilzadeh:** Formal analysis. **Mohammad Hossein Ghahremani:** Conceptualization, Supervision. **Sandro Carrara:** Data curation. **Yadollah Omidi:** Conceptualization, Data curation, Supervision, Writing - review & editing.

Acknowledgments

The authors would like to acknowledge the International Campus of Tehran University of Medical Sciences (TUMS), Tehran, Iran for financial support (grant#: 94-03-103-29923). This research was a part of Ph.D. project number 9123641001 of TUMS and performed at the Research Center for Pharmaceutical Nanotechnology (RCPN) at Tabriz University of Medical Sciences (Tabriz, Iran).

Appendix A. Supplementary data

Supplementary data to this article can be found online at https://doi.org/10.1016/j.bios.2019.111439.

References

Afsharan, H., Navaeipour, F., Khalilzadeh, B., Tajalli, H., Mollabashi, M., Ahar, M.J., Rashidi, M.-R., 2016. Biosens. Bioelectron. 80, 146–153.
Ahmad, K., Mobin, S.M., 2019. Mater. Res. Express 6, 085508.
Ahmad, K., Mohammad, A., Mathur, P., Mobin, S.M., 2016. Electrochim. Acta 215, 435–446.
Akbari Nakhjavani, S., Khalilzadeh, B., Samadi Pakchin, P., Saber, R., Ghahremani, M.H., Omidi, Y., 2018. Biosens. Bioelectron. 122, 8–15.
Aktas, B., Kasimir-Bauer, S., Muller, V., Janni, W., Fehm, T., Wallwiener, D., Pantel, K., Tewes, M., 2016. BMC Canc. 16, 1–8.
Aliakbarinodehi, N., De Micheli, G., Carrara, S., 2016. Anal. Chem. 88, 9347–9350.
Aliakbarinodehi, N., Stradolini, F., Nakhjavani, S.A., Tzouvadaki, I., Taurino, I., De Micheli, G., Carrara, S., 2018. IEEE Sens. J. 18, 5073–5081.
Aslan, S., Anik, Ü., 2014. Electroanalysis 26, 1373–1381.
Babamiri, B., Salimi, A., Hallaj, R., 2018. Biosens. Bioelectron. 102, 328–335.
Bray, F., Ferlay, J., Soerjomataram, I., Siegel, R.L., Torre, L.A., Jemal, A., 2018. CA A Cancer J. Clin. 68, 394–424.
Cao, J.T., Yang, J.J., Zhao, L.Z., Wang, Y.L., Wang, H., Liu, Y.M., Ma, S.H., 2018. Biosens. Bioelectron. 99, 92–98.
Dresselhaus, M.S., Jorio, A., Hofmann, M., Dresselhaus, G., Saito, R., 2010. Nano Lett. 10, 751–758.
Jiang, W., Liu, L., Zhang, L., Guo, Q., Cui, Y., Yang, M., 2017. Microchim. Acta 184, 4757–4763.
Khalilzadeh, B., Hasanzadeh, M., Sanati, S., Saghatforoush, L., Shadjou, N., Dolatabadi,

J.E.N., Sheikhzadeh, P., 2011. Int. J. Electrochem. Sci. 6, 4164–4175.
Khalilzadeh, B., Rashidi, M., Soleimanian, A., Tajalli, H., Kanberoglu, G.S., Baradaran, B., Rashidi, M.-R., 2019. Int. J. Biol. Macromol. 134, 695–703.
Khalilzadeh, B., Shadjou, N., Afsharan, H., Eskandani, M., Charoudeh, H.N., Rashidi, M.-R., 2016. Bioimpacts 6, 135–147.
Khalilzadeh, B., Shadjou, N., Eskandani, M., Charoudeh, H.N., Omidi, Y., Rashidi, M.-R., 2015. RSC Adv. 5, 58316–58326.
Kim, S.K., Kim, D., Jeon, S., 2012. Sensor. Actuator. B Chem. 174, 285–291.
Li, N., Wang, Y., Cao, W., Zhang, Y., Yan, T., Du, B., Wei, Q., 2015. J. Mater. Chem. B 3, 2006–2011.
Li, Y., Yang, W.K., Fan, M.Q., Liu, A., 2011. Anal. Sci. 27, 727–731.
Lv, H., Li, Y., Zhang, X., Gao, Z., Zhang, C., Zhang, S., Dong, Y., 2018. Biosens. Bioelectron. 112, 1–7.
Marcano, D.C., Kosynkin, D.V., Berlin, J.M., Sinitskii, A., Sun, Z., Slesarev, A., Alemany, L.B., Lu, W., Tour, J.M., 2010. ACS Nano 4, 4806–4814.
Mohammad, A., Ahmad, K., Qureshi, A., Tauqeer, M., Mobin, S.M., 2018. Sensor. Actuator. B Chem. 277, 467–476.
Mulfinger, L., Solomon, S.D., Bahadory, M., Jeyarajasingam, A.V., Rutkowsky, S.A., Boritz, C., 2007. J. Chem. Educ. 84, 322.
Norouzi, P., Gupta, V.K., Faridbod, F., Pirali-Hamedani, M., Larijani, B., Ganjali, M.R., 2011. Anal. Chem. 83, 1564–1570.
Ogoshi, K., Mitomi, T., 1984. Gan No Rinsho 30, 1913–1918.
Orjasaeter, H., Staab, H.J., Heier, H.E., Hornung, A., Kjorstad, K., Luedin, E., Rognum, T.O., Bell, H., 1985. NIPH (Natl. Inst. Public Health) Ann. (Oslo) 8, 13–26.
Orth, E.S., Fonsaca, J.E.S., Domingues, S.H., Mehl, H., Oliveira, M.M., Zarbin, A.J.G., 2013. Carbon 61, 543–550.
Pakchin, P.S., Nakhjavani, S.A., Saber, R., Ghanbari, H., Omidi, Y., 2017. Trends Anal. Chem. 92, 32–41.
Rahmanian, N., Eskandani, M., Barar, J., Omidi, Y., 2017. J. Drug Target. 25, 202–215.
Rojas, K., Stuckey, A., 2016. Clin. Obstet. Gynecol. 59, 651–672.
Roy, S., Soin, N., Bajpai, R., Misra, D.S., McLaughlin, J.A., Roy, S.S., 2011. J. Mater. Chem. 21, 14725–14731.
Samadi Pakchin, P., Ghanbari, H., Saber, R., Omidi, Y., 2018. Biosens. Bioelectron. 122, 68–74.
Shao, Y., Sun, X., He, Y., Liu, C., Liu, H., 2015. PLoS One 10, 1–11.
Song, K., Ding, C., Zhang, B., Chang, H., Zhao, Z., Wei, W., Wang, J., 2018. Mikrochim. Acta 185, 310.
Song, Y., Luo, Y., Zhu, C., Li, H., Du, D., Lin, Y., 2016. Biosens. Bioelectron. 76, 195–212.
Stieber, P., Nagel, D., Blankenburg, I., Heinemann, V., Untch, M., Bauerfeind, I., Di Gioia, D., 2015. Clin. Chim. Acta 448, 228–231.
Svobodova, S., Kucera, R., Fiala, O., Karlikova, M., Narsanska, A., Zednikova, I., Treska, V., Slouka, D., Rousarova, M., Topolcan, O., Finek, J., 2018. Anticancer Res. 38, 465–469.
Thompson, J.A., Grunert, F., Zimmermann, W., 1991. J. Clin. Lab. Anal. 5, 344–366.
Torrente-Rodríguez, R., Campuzano, S., López-Hernández, E., Montiel, V.R.-V., Barderas, R., Granados, R., Sánchez-Puelles, J.M., Pingarrón, J., 2015. Biosens. Bioelectron. 66, 385–391.
Tzouvadaki, I., Aliakbarinodehi, N., Dávila Pineda, D., De Micheli, G., Carrara, S., 2018. Sensor. Actuator. B Chem. 262, 395–403.
Vandghanooni, S., Eskandani, M., Barar, J., Omidi, Y., 2018. Nanomedicine 13, 2729–2758.
Wu, S.G., He, Z.Y., Zhou, J., Sun, J.Y., Li, F.Y., Lin, Q., Guo, L., Lin, H.X., 2014. Breast 23, 88–93.
Wu, T.L., Sun, Y.C., Chang, P.Y., Tsao, K.C., Sun, C.F., Wu, J.T., 2003. J. Clin. Lab. Anal. 17, 241–246.
Xu, T.-S., Li, X.-Y., Xie, Z.-H., Li, X.-G., Zhang, H.-Y., 2015. Microchim. Acta 182, 2541–2549.
Yang, Z., Lan, Q., Li, J., Wu, J., Tang, Y., Hu, X., 2017. Biosens. Bioelectron. 89, 312–318.
Zaleski, M., Kobilay, M., Schroeder, L., Debald, M., Semaan, A., Hettwer, K., Uhlig, S., Kuhn, W., Hartmann, G., Holdenrieder, S., 2018. Oncotarget 9, 22523–22536.
Zehentner, B.K., Carter, D., 2004. Clin. Biochem. 37, 249–257.
Zeng, S., Yong, K.T., Roy, I., Dinh, X.Q., Yu, X., Luan, F., 2011. Plasmonics 6, 491–506.
Zhang, H., Cui, H., 2009. Langmuir 25, 2604–2612.
Zhang, L., Wang, Y., Shen, L., Yu, J., Ge, S., Yan, M., 2017. Analyst 142, 2587–2594.
Zhao, J., Zhang, Y., Li, H., Wen, Y., Fan, X., Lin, F., Tan, L., Yao, S., 2011. Biosens. Bioelectron. 26, 2297–2303.
Zhu, C., Du, D., Lin, Y., 2017. Biosens. Bioelectron. 89, 43–55.
Zhu, Q., Chai, Y., Zhuo, Y., Yuan, R., 2015. Biosens. Bioelectron. 68, 42–48.